Hierarchical Structure in Oriented Fibers of a Dendronized Polymer

Shu Feng,[†] Xingquan Xiong,[‡] Guoliang Zhang,[†] Nan Xia,[†] Yongming Chen,*[,‡] and Wei Wang*[,†]

Key Laboratory of Functional Polymer Materials of Ministry of Education and Institute of Polymer Chemistry, College of Chemistry, Nankai University, Tianjin 300071, China, and State Key Laboratory of Polymer Physics and Chemistry, Joint Laboratory of Polymer Science and Material, Institute of Chemistry, Chinese Academy of Sciences, Beijing 100190, China

Received July 15, 2008; Revised Manuscript Received November 6, 2008

ABSTRACT: Herein we report the fabrication and study of hierarchically structured fibers of a dendronized polymer that were simply prepared by drawing out from their columnar phase in melt. At first, the combined SEM and SAXS results indicate that the fibers contain fibrils that align along the axial direction and have a diameter of ∼200 nm. Further SAXS characterizations confirm an oriented hexagonally packed cylindrical (HPC) structure assembling in the fibrils. At the molecular level, a wormlike single molecular conformation was visualized by AFM, indicating its relatively stiffer structure compared with conventional polymers. Because of this feature, the dendronized polymer can be fabricated into fibers with a highly ordered structure. Therefore, the hierarchical structure that is found in the fibers sheds light on the possible mechanism of the self-organization of the dendronized polymer on different scales.

Introduction

The investigation and fabrication of hierarchically structured materials that mimic the multiordered architectures observed in the biomaterials have aroused numerous research interests.[1−4] Many natural or synthetic materials exhibit structures of more than one length scale ranging from the nanoscale to the macroscale.[1,2,5−8] These studies have demonstrated that the structural hierarchy can play a key role in determining the physical properties of the bulk materials and their special applications.[2,9−11] These materials include biological materials such as wood and tendons,[1,2,12−14] synthetic organic materials such as dendrons[8,15−19] and macrocyclic molecules,[20−22] and inorganic materials such as polycrystals and metal oxides.[2]

Among polymeric materials, synthetic fibers such as nylon and polypropylene have attracted extensive attention and have been widely used in past decades. Currently, it is clear that the highly oriented and hierarchical structures of long chain macromolecules created by an exterior force field are the key factors that govern their mechanical properties along the axial direction.[23−25] It has been found that some rodlike macromolecules can be spun into high-performance fibers with hierarchical and highly oriented structures from the lyotropic or thermotropic liquid-crystal (LC) phase. Among them, Kevlar by Dupont and Twaron by Teijin prepared from the lyotropic LC phase of poly(*p*-phenylene terephthalamide) are the famous examples.[26]

In recent years, more and more efforts have been extended to employ soft materials in the construction of functional materials with hierarchical structures. Among these soft materials, dendronized polymers can form a cylindrical supramolecular structure in which the central backbone is jacketed by the fan-shaped monodendrons in melt. More interestingly, they can exhibit fascinating liquid-crystalline (LC) behavior[27−29] and hierarchical structure in the spatial ranging from several nanometers to several hundred nanometers.[8,15−18,30] So far, extensive emphasis was placed on synthesizing new dendronized polymers with special functionality. Herein we report the fabrication and study of hierarchically structured fibers of a dendronized polymer that were prepared by a simple drawing in their columnar phase. Hierarchical structures found in the drawn fibers were formed through multiordered organizations of the dendronized polymers from the wormlike single cylinders to the oriented and hexagonally packed cylindrical (HPC) structure and finally to the fibrillar structure. The main aim of this research is to get an understanding of the structure and morphology of the fibers prepared from dendronized polymers from the viewpoint of polymer materials science and, therefore, to widen the scope of their potential application considerably.

Experimental Section

Materials. The molecular structure of the dendronized polymer is shown in Scheme 1. This codendronized polymer was prepared by direct radical copolymerization of maleimide pendent with polyester dendron and styrene pendent with Percec-type polyether dendron. The detailed synthesis of this compound has been reported in our previous work.[31] Its weight-average molecular weight is $\bar{M}_w = 7.08 \times 10^5$ g/mol, and the polydispersity index (PDI) is $\bar{M}_w/M_n = 1.30$.

Scheme 1. Chemical Structure of the Codendronized Polymer

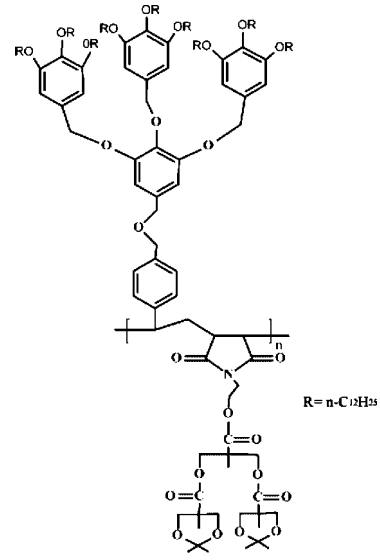

* Corresponding authors. E-mail: ymchen@iccas.ac.cn (Y.C.); weiwang@nankai.edu.cn (W.W.).
[†] Nankai University.
[‡] Chinese Academy of Sciences.

10.1021/ma8015932 CCC: $40.75
Published on Web 12/12/2008

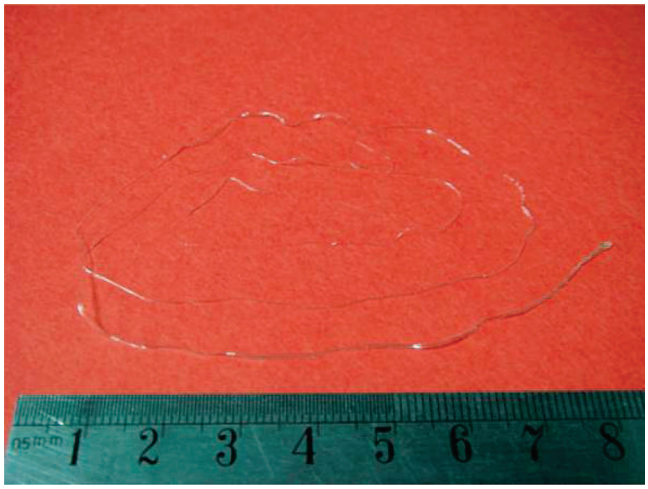

Figure 1. Fiber of this dendronized polymer prepared by drawing.

Preparation of Fiber Samples. The fiber samples can be prepared simply by drawing the LC melt of this codendronized polymer. In our experiment, we found that the best fiber could be drawn using a pair of tweezers from the melt on a hot stage, which was present at 90 °C. Normally, the fiber length can be as long as a couple tens of centimeters, as shown in Figure 1.

Analysis and Characterization Techniques. *Scanning Electron Microscopy (SEM).* We prepared the samples for SEM characterization by peeling the fibers in liquid nitrogen and then sputtering them with a thin layer of Au to avoid changing effect. For SEM observation, a LEO 1530VP field emission scanning electron microscope operated at 2 kV was used in this study.

Polarized Optical Microscopy (POM). Birefringence of the fiber samples was investigated using an optical microscope (Olympus BX51) with and without crossed polarizers. The optical microscope was equipped with an Olympus digital compact camera.

Small-Angle X-ray Scattering (SAXS). SAXS experiments were performed using SAXS equipment with a 2D detector (Brucker Histar) and were operated at 40 kV and 35 mA. The wavelength of the incident X-ray beam from Cu Kα radiation was $\lambda = 0.154$ nm. The distances between the sample and the detector were 274 and 1200 mm, respectively. In this work, the scattering intensity (I) as a function of the scattering vector (q), where $q = 4\pi(\sin\theta/\lambda)$ and 2θ is the scattering angle, or an azimuthal angle (φ) was determined from the 2D scattering patterns using the software provided by the manufacturer. The periodic structure was determined from the position of peak maxima in I versus q curves. The oriented structure was determined from azimuthal profiles (or I vs φ curves) of the strongest peak.

Atomic Force Microscopy (AFM). Samples for single molecular conformation were prepared by solvent casting at ambient temperature by spin coating the dilute THF solutions (1×10^{-5} g/mol) on a freshly cleaved highly oriented pyrolytic graphite (HOPG). The samples were analyzed after complete evaporation of the solvent at room temperature. All AFM images were recorded under air with a multimode atomic force microscope (AFM, Digital Instrumental Nanoscope IV) operated in tapping mode. The probes were commercially available silicon tips with a spring constant of 40 N·m^{-1}. In this work, both the height and the phase signal images were recorded with the highest sampling resolution available, that is, 512 × 512 pixels.

Tensile Testing. The tensile test was performed on a tensile testing device (LLA-06A, China) fitted with fiber fixtures. The specimens of 10 mm length were tested at a speed of 2 mm/min. The diameters of the fiber samples were measured using an optical microscope.

Results and Discussion

Hexagonally Packed Cylindrical Structure in Melt. Figure 2a shows the 2D SAXS pattern obtained from a sample frozen from the melt. The two relatively strong scattering rings indicate that no significantly aligned supramolecular structure formed in the melt. Figure 2b shows the corresponding intensity profile as a function of the scattering vector, q. The first sharp peak centered at $q_1 = 1.13$ nm^{-1} appears together with a second reflection at $q_2 = 1.96$ nm^{-1}. Because $q_2/q_1 = \sqrt{3}$, the observed scattering feature is associated with the hexagonally packed cylinders. Therefore, the Miller indices, corresponding to two

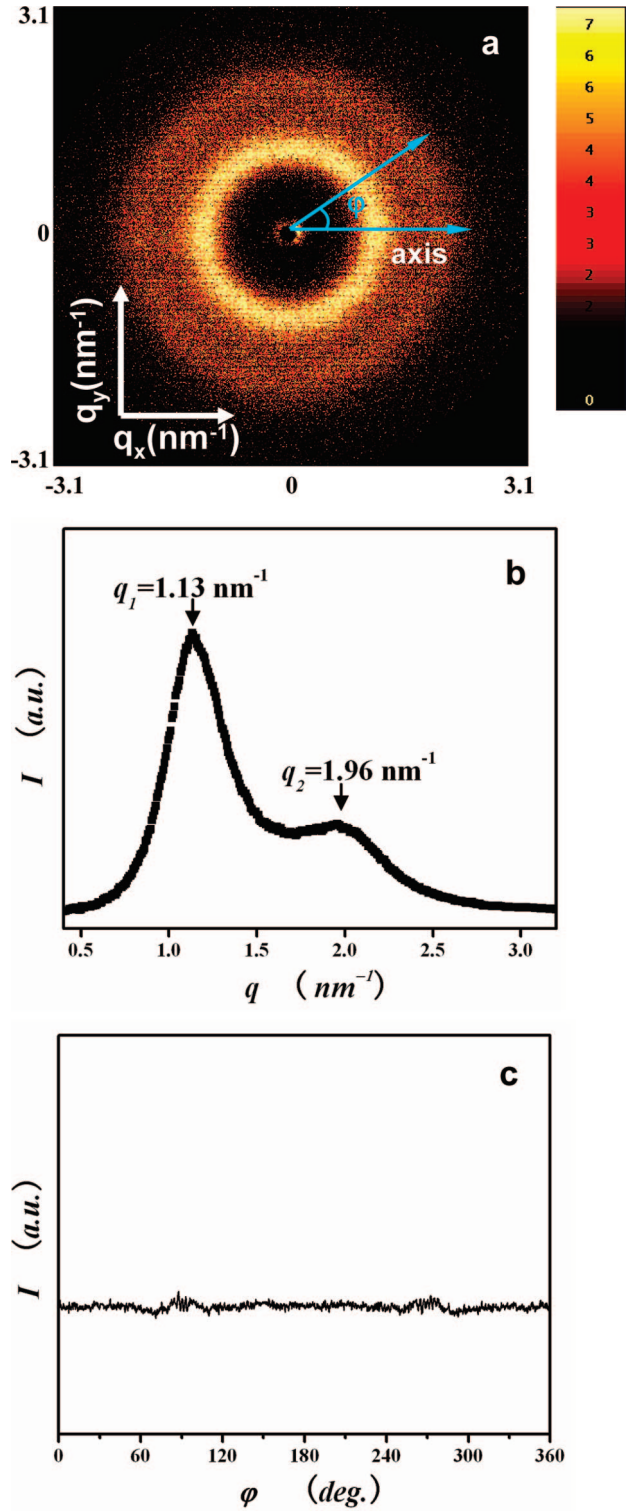

Figure 2. (a) 2D SAXS scattering pattern of a sample frozen from the melt. (b) Plot of the SAXS intensity, I, as a function of scattering vector, q. (c) Plot of the SAXS intensity, I, as a function of the azimuthal angle, φ.

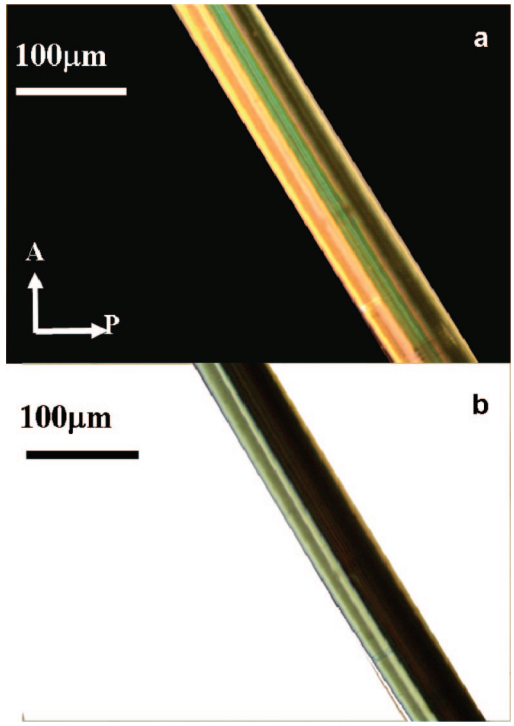

Figure 3. Optical images of a fiber. The images were taken (a) with and (b) without crossed polarizers.

scattering peaks, are (10) and (11), respectively. The diameter of the cylinders is 6.64 nm. This cylinder diameter is significantly large because the diameter of most dendronized polymers is in range of 3 to 5 nm.[8,15−18,29] First, it is important to point out the chemical structure feature of this dendronized polymer: It is composed of second-generation polyester dendrons and second-generation Percec-type dendrons. These dendrons arrange alternatively along the polymer backbone. (See Scheme 1.) In our previous work,[31] a core−shell model was suggested to describe the feature of individual cylinders in bulk samples: The core is composed of polyester dendrons, and the shell is constructed by Percec-type dendrons and long alkyl chains together.[32] Owing to these features, the cylinder diameter is larger than those of other dendronized polymers. Another possible reason is that the cylinders may be constructed by a few macromolecules, as suggested by Percec and coworkers.[33−35]

Figure 2c shows an azimuthal profile of the first scattering intensity in the range of the scattering vector of $0.85 \leq q \leq 1.56$ nm^{-1}. No change was found in the azimuthal angle (φ), $0 \leq \varphi \leq 2\pi$. This means that the subscale organization of the dendronized polymer has existed before drawing but within random distributed orientations.

Formation of the Fibers. Fibers of this polymer were prepared by drawing the polymer from its columnar phase at 90 °C. The fiber length can be ∼45 cm. (See Figure 1.) Figure 3a,b shows optical micrographs of a fiber taken with and without crossed polarizers, respectively. The fiber diameter is ∼100 μm. Under the crossed polarizers, the fiber exhibits a strong birefringence that indicates the formation of the oriented structure. Figure 4 shows an SEM image of a fiber. The fiber with a ∼100 μm diameter has a smooth surface.

Oriented Fibrils. SEM observation on a laterally fractured surface of the fibers created by the peeling technique in liquid nitrogen can give more structural information on the interior of a fiber. A typical SEM image of the peeled fibers is shown in Figure 5. There are fibrils extending parallel to the fiber axis,

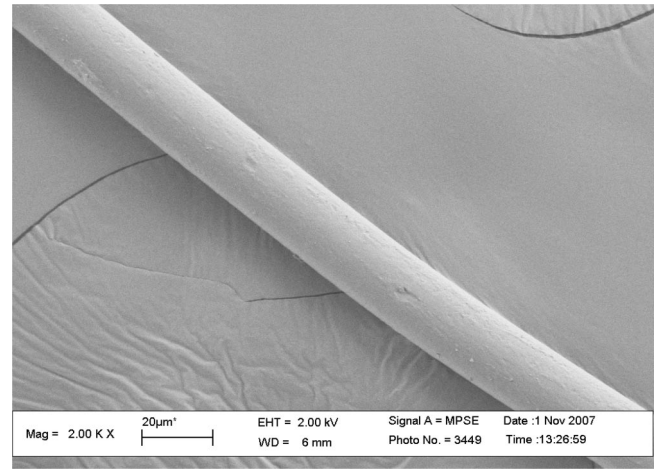

Figure 4. SEM image of a fiber surface.

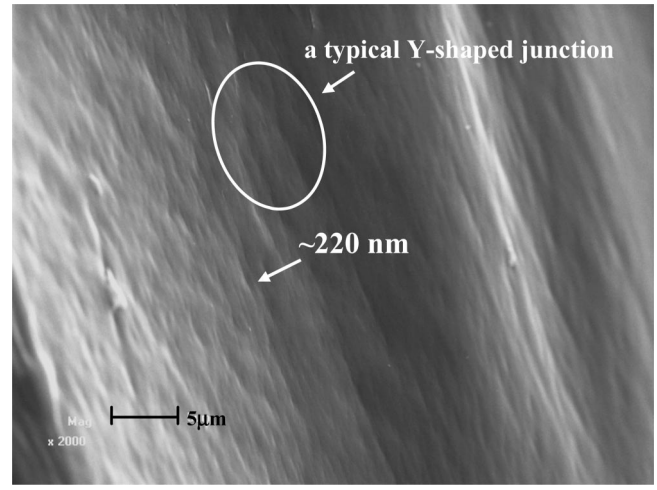

Figure 5. SEM image of the laterally fractured surface showing the internal fibrillar structure.

and their diameter is ∼220 nm. Furthermore, a longitudinal substructure of the typical Y-shaped junctions between the fibrils can also be observed in Figure 5, for instance, in the area marked by a ring. This means that a fibrillar network can form. However, it is difficult to determine the length of the fibrils between two junctions from this micrograph.

Figure 6a shows the 2D SAXS patterns of the fiber samples at $0 \leq q \leq 0.99$ nm^{-1} that come from some substructures. The fiber axis is indicated by the arrow in the Figure. This is a typical scattering pattern of oriented fiber samples with a larger substructure. The intensity is concentrated on a streak along the equator, which means the substructure is oriented along the fiber axis direction.[36−38] Figure 6b,c shows the typical distribution of the scattering intensity (I) as a function of the scattering vector (q) and the azimuthal angle (φ) for constant $q = 0.18$ nm^{-1}, respectively. The further analyses on I versus q and I versus φ data can provide the information of the size and orientation of substructure objects (or fibrils) in the fiber.

At first, according to Porod's law, a plot of $q^3I(q)$ as a function of q^3 is expected to be linear at the large values of q, as shown in Figure 7. This demonstrates that the electron density within the fibrils is homogeneous either within the cross-section (2D) or in all directions (3D) and that the interfacial boundaries are sharp.[39] Thus, the scattering intensity, $I(q)$, can be described as

$$I(q) = K_p q^{-3} + I_{Fl} \quad (1)$$

where K_p is the Porod constant for an ideal two-phase system, and I_{Fl} is the intensity of the correction due to 2D or 3D electron density fluctuations. In Figure 7, a plot of $q^3 I_p$ versus q^3 is also given, where $I_p(q)$ is defined by $I_p(q) = I(q) - I_{Fl}$, that is, the intensity of the ideal two-phase system that is possibly composed of polymer and air that is trapped in microcavities in fibers.[36−38]

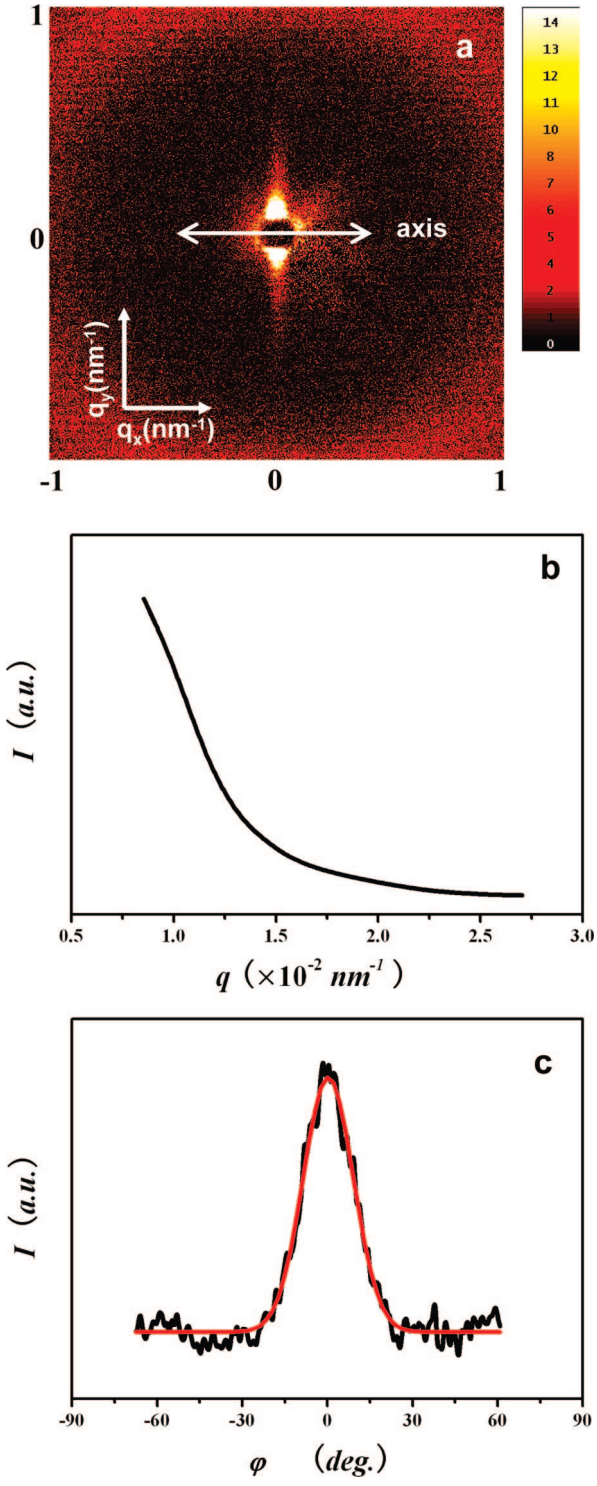

Figure 6. (a) 2D scattering pattern of the oriented fiber sample showing the scattering signals in small q regime ($0 \le q \le 0.99$ nm^{-1}). The arrows point out the fiber axis. (b) Plot of the scattering intensity $I(q)$ versus q for the fiber. (c) Typical distribution of the scattering intensity as a function of the angle φ for constant $q = 0.18$ nm^{-1}. The red curve is the fitting result using the Gaussian function.

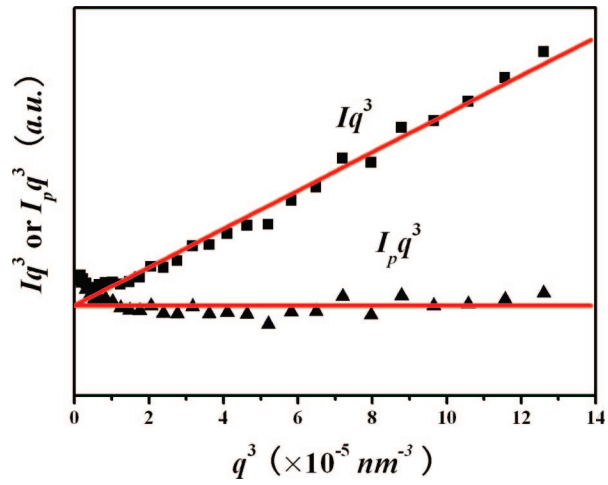

Figure 7. Plots of Iq^3 and $I_p q^3$ versus q^3 for the fiber to detect Porod's law.

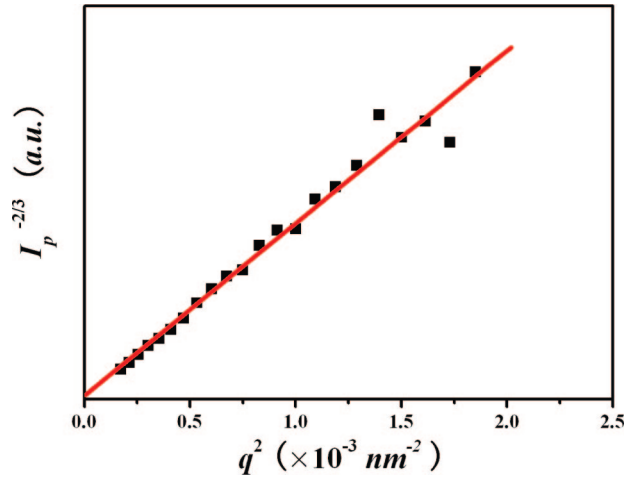

Figure 8. Determination of the average diameter of the fibrils according to the Debye method.

In this work, we applied Debye's method[40,41] to analyze the diameter of the structural units in the fibers. Therefore, the scattering intensity, $I(q)$, of the fiber samples is given as follows[41]

$$I(q) = \int \gamma(r) J_0(qr) r \, dr \quad (2)$$

where $\gamma(r)$ is a correlation function and $J_0(qr)$ is the zeroth-order Bessel function. A common correlation function is the exponential given in eq 3

$$\gamma(r) = \exp(-r/l_c) \quad (3)$$

where the variable l_c is the correlation length of the substructure along the fiber radial direction. Performing the integration in eq 2 with eq 3 yields the following result

$$I_p(q) = \frac{K l_c^2}{(1 + l_c^2 q^2)^{3/2}} \quad (4)$$

where K is a constant. For a system that follows this functional form, the correlation length can be determined from the intercept and slope of a plot of $I_p^{-2/3}$ versus q^2, as shown in Figure 8. The correlation lengths (the average diameter of the fibrils) are ~200 nm. This value is of the same order as the width measured for the fibrils with the SEM that will be discussed below. It

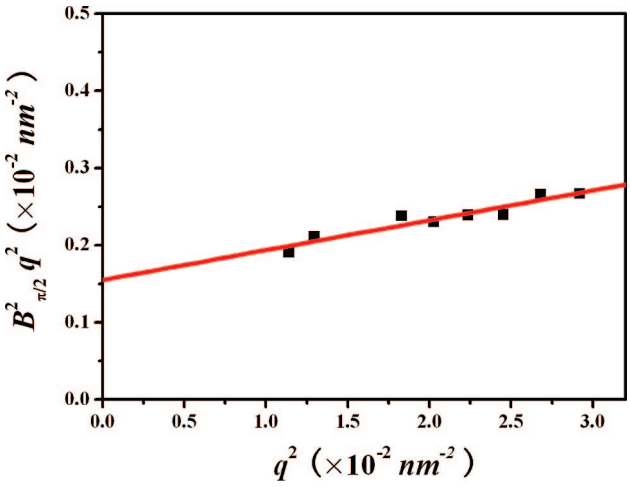

Figure 9. Plot of $q^2B^2_{\pi/2}$ versus q^2 obtained from the SAXS data in Figure 6b. According to the Ruland method, we obtained $B_{eq} = 12.5 \pm 1.5°$.

should be remembered, however, that the determined correlation length is very sensitive to small variations in the data, the scatter of the data, and any errors in determining the correction for electron density fluctuation.

We also followed the method that has been developed by Ruland[36−38] for calculating the orientation distribution of the fibrils

$$q^2B^2_{\pi/2} = 4\pi^2/L^2_{app} + q^2B^2_{eq} \quad (5)$$

where $B_{\pi/2}$ is the integral width of the angular distribution of the scattering intensity, B_{eq} is the true width of the orientation distribution, and L_{app} is the apparent length of the structure units in the direction of the fiber axis. $B_{\pi/2}$ can be obtained by fitting the azimuthal angle distribution of intensity (that is, I vs φ curve) at $-2/\pi \le \varphi \le 2/\pi$ at different q values. Figure 6c shows a fitting result using the Gaussian function at $q = 0.18$ nm^{-1}. $B_{\pi/2}$ is the full width at half-maximum (fwhm). The relationship between $q^2B^2_{\pi/2}$ and q^2 is linear, as can be seen in Figure 9. To determine B_{eq}, we fitted the data using a linear least-squares fitting routine. From the slope, we obtained $B_{eq} = 12.5 \pm 1.5°$, which means that the fibrils aligned well along the axial direction.

Oriented Hexagonally Packed Cylindrical Structure in Fibrils. Figure 10a shows another typical 2D SAXS pattern of the fibers on a larger scale ($0 \le q \le 3.1$ nm^{-1}). The arrow in the Figure indicates the fiber axis. The most interesting feature of this 2D SAXS pattern is that two bright arcs appear in the direction perpendicular to the fiber axis. This is clear evidence of the smaller structure also being oriented along the axis direction of the fibers. The corresponding intensity curve as a function of the scattering vector (q) is shown in Figure 10b. There are still two scattering peaks with $q_1 = 1.16$ nm^{-1} and $q_2 = 2.03$ nm^{-1}. Their ratio is still $q_2/q_1 \approx \sqrt{3}$, meaning that the HPC structure does not change after drawing into fibers. The azimuthal intensity distribution of the SAXS pattern, which corresponded to a Miller index of (110), was determined at $0.85 \le q \le 1.56$ nm^{-1}, as shown in Figure 10c. Therefore, this azimuthal profile suggests that the HPCs are oriented along the fiber axis.

It is well known that the orientational order parameter, $\langle \bar{P}_2 \rangle$, is a measurement of the distribution of molecular orientations around the director.[42,43] Values range between 0 and 1, where the former corresponds to an isotropic structure and the latter represents perfect alignment along the director. In this work, we used the azimuthal profile in Figure 10c to

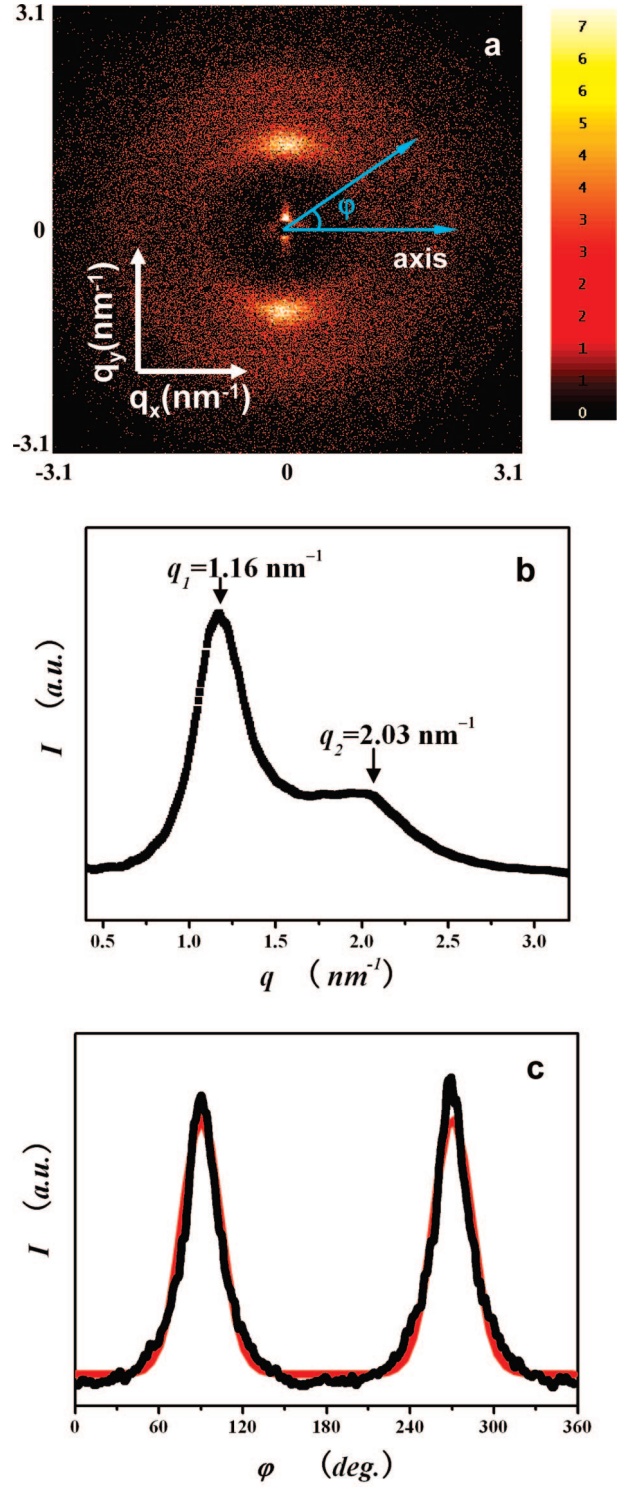

Figure 10. (a) 2D SAXS pattern of a fiber. The fiber axis is indicated by the arrow. (b) SAXS intensity, I, as a function of the scattering vector, q. (c) Azimuthal profile of the SAXS pattern scattering intensity. The red curve is the fitting result using eq 6.

calculate the orientational order parameter of the oriented HPCs. At first, the intensity profiles of an azimuthal peak can be fitted to a Maier−Saupe distribution function[44] with a free baseline (I_0) and position of the maximum (φ_0)

$$I = I_0 + Ae^{\alpha\cos^2(\phi-\phi_0)} \quad (6)$$

where φ is the azimuthal angle and α is a parameter that determines the width of the distribution. The solid curve

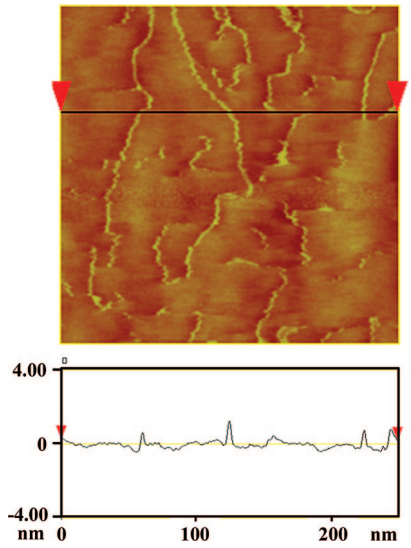

Figure 11. (a) AFM phase image of individual molecules of the dendronized polymer deposited on HOPG surface. (b) Cross-section profile, which was taken along the black line in a.

represents the fitting results. In this work, $\alpha = 9.54$. From the α parameter, the orientational order parameter $\langle \bar{P}_2 \rangle$ is determined using[45,46]

$$\overline{\langle P_2 \rangle} = \frac{\int_{-1}^{1} P_2(\cos\phi)\, e^{\alpha\cos^2\phi}\, d\cos\phi}{\int_{-1}^{1} e^{\alpha\cos^2\phi}\, d\cos\phi} \tag{7}$$

where $P_2(\cos\varphi)$ is the second-order Legendre polynomial of $\cos\varphi$

$$P_2(\cos\phi) = \frac{1}{2}(3\cos^2\phi - 1) \tag{8}$$

Equation 7 can be solved by a numerical integration. In this work, we found a relatively higher value of $\langle \bar{P}_2 \rangle = 0.83$ for the drawn fiber of the dendronized polymer, which further indicates the formation of the highly oriented structure of supramolecular cylinders of the dendronized polymer with a hexagonal arrangement. From eq 8, we obtain $\varphi \approx 18°$.

Single Molecular Conformation. Imaging individual synthetic macromolecules has become a significant focus for bringing about a better understanding of the macromolecular structure and the conformation on substrates as well as their self-assembled motifs. With samples spin casted from dilute solution ($c = 1 \times 10^{-5}$ g/mol), individual molecules could be imaged by AFM. The micrograph in Figure 11 shows a wormlike single molecular morphology of this dendronized polymer. The average width of macromolecules observed in a single layer is ~8 to 9 nm, and the height is $\sim 2.0 \pm 0.2$ nm.[47] Clearly, in contrast with conventional macromolecules, this dendronized polymer experiences steric repulsions due to densely grafted side chains. Therefore, the rigidification of the backbone by means of dendron attachment, which increases with increasing dendron generation, leads to this dendronized polymer exhibiting an extended or wormlike chain conformation. A great number of other kinds of dendronized polymers also exhibit similar structures, as reported in previous work.[18,48,49] It is the relative rigidity of this dendronized polymer that results in the formation of the hexagonally packed columnar phase from which we can prepare the fiber samples.

Suggested Model of Hierarchical Structure. In Scheme 2, we gave a schematic illustration of the hierarchical structure from single cylinder to the fibers. The existence of three orders

Scheme 2. Schematic Illustration of the Hierarchical Structure of the Fibers

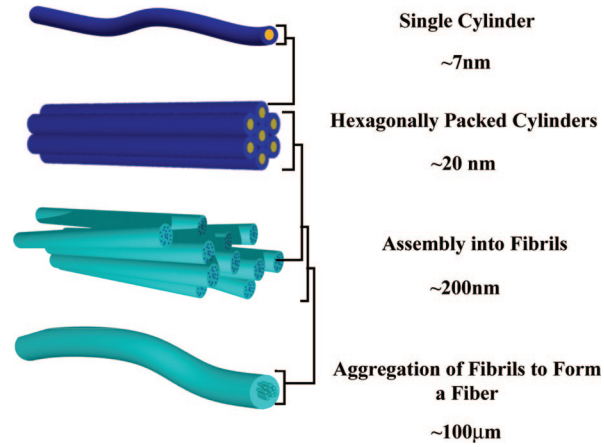

of substructures in the fiber indicates the bottom-up self-assembly process of the dendronized polymer before and (or) during drawing. Because of fan-shaped and dendritic side groups, one or a few molecules favor to form supramolecular cylinders with a wormlike conformation and a diameter of ~6.64 nm. This is the most basic physical structure of the dendronized polymers. These individual cylinders hexagonally pack to form a substructure on a scale of tens of nanometers. During the drawing, the elongation force results in an oriented arrangement of all HPCs along the fiber axis. The HPCs further construct the oriented fibrils with an average diameter of ~200 nm in the fibers. The fibrils are significantly networked because the network ensures the structural continuity along directions perpendicular as well as parallel to the fiber axis. On the basis of this hierarchical model, we come to a rational conclusion that the misorientation of the individual cylinders should be slightly higher than that of fibrils. This is because there is a misorientation of HPCs in the fibrils. Therefore, we can understand why the misorientation degree of the fibrils is ~12°, whereas the value of the HPCs is ~18°.

Tensile Properties. A typical stress−strain curve of those fibers, measured at a speed of 2 mm/min using a test length of 10 mm, is shown in Figure 12. The fibers do not exhibit the long necking phenomenon but rather pass through the yield point and steadily proceed up to the fracture point. Mechanical properties of four fibers are presented in Table 1. The mechanical properties of the fiber are relatively poor in comparison

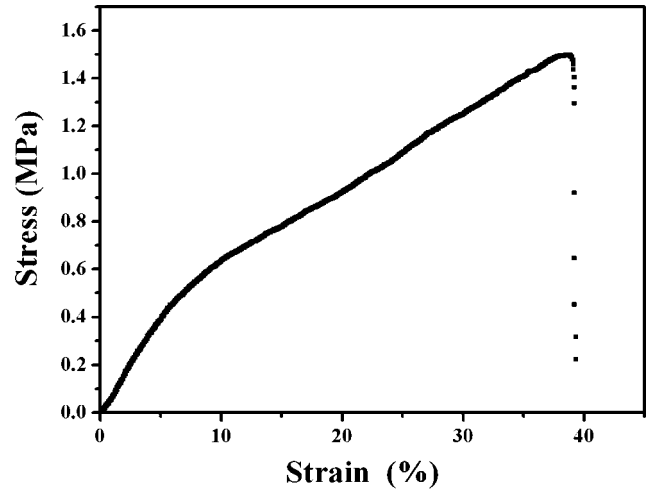

Figure 12. Typical stress−strain curve for the fibers formed by this dendronized polymer.

Table 1. Mechanical Properties of the Fibers Formed by This Dendronized Polymer

fiber no.	Young's modulus (MPa)	tensile strength (MPa)	elongation at break (%)
1	7.6	1.50	39
2	8.2	1.10	35
3	7.5	0.90	58
4	8.9	1.50	46
av	8.1 ±0.6	1.25 ±0.30	45 ± 10

with those of conventional synthetic fibers. As we all know, the tensile properties of a polymer fiber are governed by many factors, such as the manufacturing process, the kinds of materials, the fibril orientation and so on. Considering those factors, a further step, for example, changing the kinds of dendronized polymers or improving the manufacturing process, could possibly result in better tensile properties.

Conclusions

We have investigated the hierarchical structure of the fibers drawn from a dendronized polymer melt. The existence of three orders of substructures in the fibers, from the wormlike single cylinders composed of one or a few macromolecules to the oriented and HPC structure and finally to the fibrillar structure, indicates the bottom-up self-assembly process of the dendronized polymer during drawing. We thus propose that the elongation force results in an oriented arrangement of all HPCs along the fiber axis, and the HPCs further construct the oriented fibrils. We hope that this research can provide a deeper understanding of structure or morphology in fibers prepared from dendronized polymers from the viewpoint of polymer materials science and open a new avenue for widening the application scope of dendronized polymers.

Acknowledgment. Financial support by the National Science Foundation of China (20534010, 20374030, 20734001, and 20625412) is greatly acknowledged. The Nankai group thanks the State Key Laboratory of Polymer Physics and Chemistry for financial support and the Beijing Synchrotron Radiation Facility (BSRF) at the Institute of High Energy Physics of the Chinese Academy of Sciences for a special grant to perform the initial SAXS experiments in the SAXS station of BSRF.

References and Notes

(1) Fratzl, P.; Weinkamer, R. *Prog. Mater. Sci.* **2007**, *52*, 1263.
(2) Lakes, R. *Nature* **1993**, *361*, 511.
(3) O'Brien, J. P.; Fahnestock, S. R.; Termonia, Y.; Gardner, K. H. *Adv. Mater.* **1998**, *10*, 1185.
(4) Hearle, J. W. S. *J. Mater. Sci.* **2007**, *42*, 8010.
(5) Akagi, K. *Polym. Int.* **2007**, *56*, 1192.
(6) Jahnke, E.; Severin, N.; Kreutzkamp, P.; Rabe, J. P.; Frauenrath, H. *Adv. Mater.* **2008**, *20*, 409.
(7) Chatterjee, T.; Mitchell, C. A.; Hadjiev, V. G.; Krishnamoorti, R. *Adv. Mater.* **2007**, *19*, 3850.
(8) Percec, V. *Philos. Trans. R. Soc. London, Ser. A* **2006**, *364*, 2709.
(9) Loyrette, H. *Gustave Eiffel*; Rizolli: New York, 1985.
(10) Nowick, A. S.; Berry, B. S. *Anelastic Relaxation in Crystalline Solids*; Academic Press: New York, 1972.
(11) Parkhouse, J. G. In *Third International Conference on Space Structure*; Nooshin, H., Ed.; Elsevier Applied Science: London, 1984.
(12) Mattheck, C. *Design in Nature: Learning from Trees*; Springer-Verlag: New York, 1998.
(13) Currey, J. D. *Bones: Structure and Mechanics*; Princeton University Press: Princeton, NJ, 2002.
(14) Fratzl, P. *Curr. Opin. Colloid Interface Sci.* **2003**, *8*, 32.
(15) Schlüter, A. D.; Rabe, J. P. *Angew. Chem., Int. Ed.* **2000**, *39*, 864.
(16) Frey, H. *Angew. Chem., Int. Ed.* **1998**, *37*, 2193.
(17) Zhang, A.; Shu, L. J.; Bo, Z. S.; Schlüter, A. D. *Macromol. Chem. Phys.* **2003**, *204*, 328.
(18) Frauenrath, H. *Prog. Polym. Sci.* **2005**, *30*, 325.
(19) Percec, V.; Ahn, C. H.; Ungar, G.; Yeardley, D. J. P.; Möller, M.; Sheiko, S. S. *Nature* **1998**, *391*, 161.
(20) Petitjean, A.; Nierengarten, H.; Dorsselaer, A. V.; Lehn, J. M. *Angew. Chem., Int. Ed.* **2004**, *43*, 3695.
(21) Schappacher, M.; Deffieux, A. *Science* **2008**, *319*, 1512.
(22) Ghosh, S.; Ramakrishnan, S. *Angew. Chem., Int. Ed.* **2005**, *44*, 5441.
(23) Viale, S.; Best, A. S.; Mendes, E.; Picken, S. J. *Chem. Commun.* **2005**, 1528.
(24) Zimmerman, J. In *Comprehensive Polymer Science: The Synthesis, Characterization, Reactions, and Applications of Polymers*; Allen, S. G., Bevington, J. C., Eds.; Pergamon Press: Oxford, 1989; Vol. *7*.
(25) *Structure and Properties of Oriented Polymers*; Ward, I. M., Ed.; Chapman & Hall: London, 1997.
(26) Kwolek, S. L.; Morgan, P. W.; Schaftgen, J. R. In *Encyclopedia of Polymer Science and Engineering*; Kroschwitz, J. I., Ed.; Wiley: New York, 1988; Vol. *9*.
(27) Canilho, N.; Kasëmi, E.; Mezzenga, R.; Schlüter, A. D. *J. Am. Chem. Soc.* **2006**, *128*, 13998.
(28) Canilho, N.; Kasëmi, E.; Schlüter, A. D.; Mezzenga, R. *Macromolecules* **2007**, *40*, 2822.
(29) Canilho, N.; Kasëmi, E.; Schlüter, A. D.; Ruokolainen, J.; Mezzenga, R. *Macromolecules* **2007**, *40*, 7609.
(30) Percec, V.; Mitchell, C. M.; Cho, W. D.; Uchida, S.; Glodde, M.; Ungar, G.; Zeng, X.; Liu, Y.; Balagurusamy, V. S. K.; Heiney, P. A. *J. Am. Chem. Soc.* **2004**, *126*, 6078.
(31) Xiong, X.; Chen, Y.; Feng, S.; Wang, W. *Macromolecules* **2007**, *40*, 9084.
(32) Because the dendrons are alternatively arranged along the backbone, we do not have experimental evidence to indicate a phase separation between the two dendrons. The suggested core−shell model means that the polyester dendrons may be located in the center of the cylinders, and Percec-type dendrons should distribute in the periphery of the cylinders because of their size and the effect of long alkyl chains. This cylinder can be formed by a single or a couple macromolecules. A further study is needed to clarify this point.
(33) Percec, V.; Rudick, J. G.; Peterca, M.; Heiney, P. A. *J. Am. Chem. Soc.* **2008**, *130*, 7503.
(34) Percec, V.; Peterca, M.; Rudick, J. G.; Aqad, E.; Imam, M. R.; Heiney, P. A. *Chem.—Eur. J.* **2007**, *13*, 9572.
(35) Percec, V.; Glodde, M.; Peterca, M.; Rapp, A.; Schnell, I.; Spiess, H. W.; Bera, T. K.; Miura, Y.; Balagurusamy, V. S. K.; Aqad, E.; Heiney, P. A. *Chem.—Eur. J.* **2006**, *12*, 6298.
(36) Ruland, W. *J. Appl. Crystallogr.* **1971**, *4*, 70.
(37) Wang, W.; Ruland, W.; Cohen, Y. *Acta Polym.* **1993**, *44*, 273.
(38) Thünemann, A. F.; Ruland, W. *Macromolecules* **2000**, *33*, 1848.
(39) Porod, G. *Kolloid-Z.* **1951**, *124*, 83.
(40) Debye, P.; Anderson, H. R.; Brumberger, H. *J. Appl. Phys.* **1957**, *28*, 678.
(41) Debye, P.; Bueche, A. M. *J. Appl. Phys.* **1949**, *20*, 519.
(42) Vainshtein, B. K. *Diffraction of X-rays by Chain Molecules*; Elsevier: New York, 1966.
(43) Gedde, U. W. *Polymer Physics*; Chapman & Hall: London, 1995.
(44) Mitchell, G. R. In *Comprehensive Polymer Science*; Allen, G.; Bevington, J. C., Eds.; Pergamon Press: Oxford, 1989; Vol. *1*.
(45) Maier, W.; Saupe, A. Z. *Z. Naturforsch., A: Astrophys., Phys., Phys. Chem.* **1961**, *16*, 816.
(46) Taylor, J. E.; Uribe, A. R.; Libera, M. R. *Polymer* **2002**, *43*, 1641.
(47) Ruijter, C. D.; Mendes, E.; Boerstoel, H.; Picken, S. J. *Polymer* **2006**, *47*, 8517.
(48) We note that on the HOPG surface, epitaxial adsorption of the peripheral alkyl tails to the HOPG surface and the broadening of the finite radius of the AFM tip itself can lead to a molecular size that is larger than the true width.
(49) Percec, V.; Rudick, J. G.; Wagner, M.; Obata, M.; Mitchell, C. M.; Cho, W. D.; Magonov, S. N. *Macromolecules* **2006**, *39*, 7342.
(50) Sheiko, S. S.; Möller, M. *Chem. Rev.* **2001**, *101*, 4099.

MA8015932